

# 80% Scaled NASA Common Research Model Wind Tunnel Test of JAXA at Relatively Low Reynolds Number

Makoto Ueno\*, Takamasa Kohzai†, Seigo Koga‡  
Hiroyuki Kato§, Kazuyuki Nakakita¶ and Norikazu Sudani||  
*Japan Aerospace Exploration Agency, Chofu, Tokyo, 182-8522, Japan*

A wind tunnel test of a 80% scaled copy of the NASA Common Research Model (CRM) was performed in the 2m × 2m transonic wind tunnel of Japan Aerospace Exploration Agency (JAXA). The wind tunnel model was fabricated by JAXA consulting NASA Langley Research Center and the Drag Prediction Workshop committee members. The test was conducted at relatively low Reynolds number of  $2.27 \times 10^6$  due to the limitation of the tunnel capability and boundary layer transition was simulated with optimized roughness.

In the test campaign, static pressure distribution and aerodynamic forces were successfully acquired while the model main wings were deformed during the test due to the dynamic pressure. To make a fair comparison with the data from other sources in different circumstances, data normalization techniques were applied. Then, the data was compared with the data of the National Transonic Facility of NASA and CFD. The data normalization successfully realized fair comparisons for pressure distribution and lift coefficients while the tests were performed at the different circumstances such as the different Reynolds numbers.

## Nomenclature

$\alpha$	Angle of attack
$\eta$	Span-wise section location normalized by the half span length $b/2$
$\Lambda_m$	Sweep of the maximum-thickness line
$(x/c)_m$	Chordwise location of the airfoil maximum thickness point
$A_{\max}$	Maximum cross sectional area of the body
$b$	Reference span length
$c$	Chord length
$c_{\text{ref}}$	Reference chord
$c_a$	2-dimensional axial force coefficient at a wing section
$c_d$	2-dimensional drag coefficient at a wing section
$C_f$	Skin friction coefficient
$c_l$	2-dimensional lift coefficient at a wing section
$c_n$	2-dimensional normal force coefficient at a wing section
$c_p$	Static pressure coefficient
$d$	Reference diameter of the body $\sqrt{(4/\pi)A_{\max}}$
$F_x, F_y, F_z, M_x, M_y$ and $M_z$	6-component force/moment
$FF$	Form factor

\*Associate Senior Researcher, Institute of Aerospace Technology, ueno.makoto@jaxa.jp, Senior Member AIAA.

†Researcher, Institute of Aerospace Technology, masataka.kohzai@jaxa.jp, Member AIAA.

‡Researcher, Institute of Aerospace Technology, seigo.koga@jaxa.jp, Non-member

§Associate Senior Researcher, Institute of Aerospace Technology, ueno.makoto@jaxa.jp, Senior Member AIAA.

¶Senior Researcher, Institute of Aerospace Technology, ueno.makoto@jaxa.jp, Senior Member AIAA.

||Senior Researcher, Institute of Aerospace Technology, ueno.makoto@jaxa.jp, Senior Member AIAA.

$l$	Length of the body
$M$	Mach number
$M_{pc}$	Mach number calculated using plenum chamber static pressure
$P_{pc}$	Plenum chamber static pressure
$P_0$	Total pressure
$Q$	Component interference factor
$Re$	Reynolds number
$Re_c$	Reynolds number based on the reference chord length $c_{ref}$
$S_{ref}$	Reference area
$t$	Thickness of the wing
$x$	x-component coordinate of body axis
$z$	z-component coordinate of body axis

## I. Introduction

DRAG prediction is a kind of the most important aspect of aerodynamics concerning commercial airplane development. Recently, there are some efforts to utilize computational fluid dynamics (CFD) to estimate drag and the AIAA have been holding the AIAA drag prediction workshops (DPW) since 2001.<sup>1,2,3,4</sup> The information about the workshop can be acquired from the [web page \(http://aac.larc.nasa.gov/tsab/cfdlarc/aiaa-dpw/\)](http://aac.larc.nasa.gov/tsab/cfdlarc/aiaa-dpw/). To ensure reliability of CFD drag prediction, assurance with wind tunnel test results are crucial. However, consistency of the results among wind tunnels might not be expected all the time, while wind tunnel testing has been conducted since very old days.

In the DPW-4 and the DPW-5, the NASA Common Research Model (CRM) is designed<sup>5</sup> and has been used as the target shape of the workshop. As the experimental reference, the NASA Langley Research Center (LaRC) fabricated the wind tunnel model and did the tests of it<sup>6,7,8,9</sup> and have been continuing further analyses.<sup>10,11</sup> Japan Aerospace Exploration Agency (JAXA) is also making an effort to predict aerodynamic characteristics consistently both by CFD and wind tunnel testing. JAXA is now attending the DPW<sup>12</sup> and fabricated a 80% scaled CRM. The wind tunnel model of JAXA was designed for its wind tunnel facility, JAXA 2m  $\times$  2m transonic wind tunnel (JTWT). Thus, a set of wind tunnel campaign has been planned and conducted.

The objectives of the wind tunnel test is to acquire stable experimental data and clarify correlation between CFD and test results of other facilities. Additionally, because the wind tunnel cannot achieve sufficiently high Reynolds number, its availability and limit to actual high Reynolds number target should be assessed. To achieve these objectives, a fair comparison of the data with that from other sources, such as other wind tunnels and CFD, should be prepared. In this article, data normalization techniques are introduced. Then, application of it and the actual comparison of the data among wind tunnels and CFD are shown.

## II. Facility and Equipments

### II.A. Wind Tunnel

The 2m  $\times$  2m transonic wind tunnel of Japan Aerospace Exploration Agency (JTWT) was used for the tests. It has 4 exchangeable rectangle test sections with the reference height and the reference width of 2 m. A test section with porous walls were used for this test campaign. The perforation holes are perpendicular to the walls and the opening ration of the wall is 20%. The total pressure and the Mach number can be controlled from 50 to 150 kPa and from 0.1 to 1.4, respectively. The wind tunnel is equipped with a 22,500 kW blower, and supersonic operation is achieved using a 8,000kW auxiliary blower. A bird's eye view of the wind tunnel is shown in Fig. 1. The Mach number is controlled with the total pressure ( $P_0$ ) and the static pressure of the plenum chamber ( $P_{pc}$ ). The Mach number calculated by the  $P_0$  and the  $P_{pc}$  is called the plenum chamber Mach number ( $M_{pc}$ ).

### II.B. Wind Tunnel Model

The wind tunnel model in use is a 80% scaled copy of the NASA Common Research Model of NASA National Transonic Facility.<sup>6</sup> It was scaled to 80% of the NTF's NASA CRM because of the test section size of the

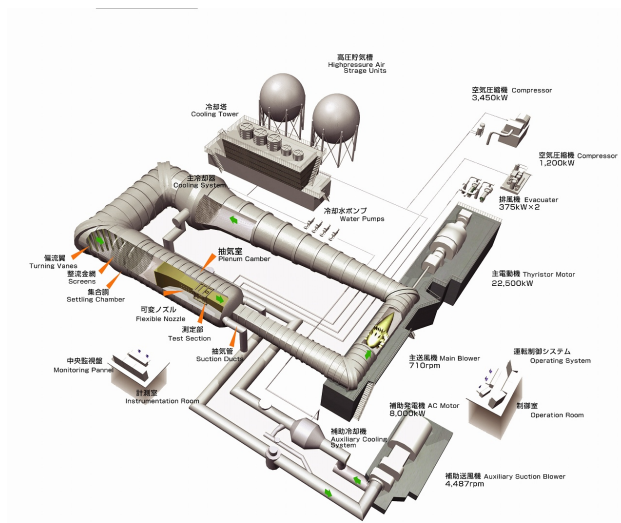


Figure 1. Bird's eye view of the JAXA 2 m × 2 m transonic wind tunnel

JTWT. Cross section images of each test section in which the model is installed are shown in Fig. 2. As seen in the figure, the relative cross sectional areas of the model are the same. The geometry of the models are tabulated in Table 1.

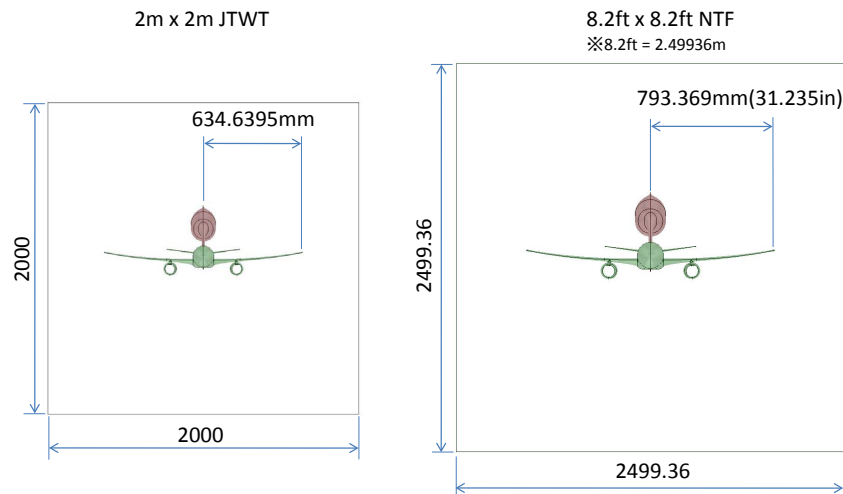


Figure 2. Cross section images of the test sections with wind tunnel models.

The model consists of a body, main wings and horizontal stabilizers. 3 deflection angles of (-2/0/2) deg of horizontal stabilizers were prepared. Covers to fill the holes of the stabilizer installation were fabricated so that a test with horizontal tails is available. Nacelles and pylons below the main wings are fabricated and they are also removable. The support sting was fabricated as a scaled copy of the sting used in the NTF test.

An image of the wind tunnel test model in the test section of the JTWT is shown in Fig. 3.

	NTF's model	JAXA's 80% scaled model
Reference Area ( $S_{\text{ref}}$ )	279709.7 mm <sup>2</sup>	179014.2 mm <sup>2</sup>
Reference Chord ( $c_{\text{ref}}$ )	189.1 mm	151.31 mm
Reference Span ( $b$ )	1586.6 mm	1269.3 mm

**Table 1. Geometry of the model.**

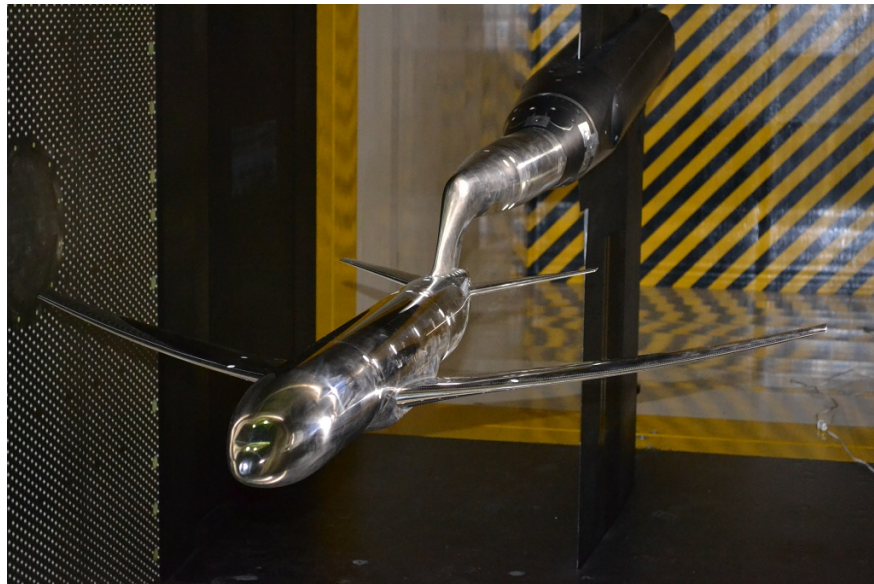


**Figure 3. Wind tunnel model in the test section of the JTWT.**

## II.C. Measurement Equipments

### II.C.1. Force and Pressure Measurements

A block diagram of the measurement system is shown in Fig. 4. All the transmission line, however, could not pass the support sting because of those thickness. Thus, the test campaign was divided in two parts such as static and unsteady measurement.

Measurement equipment prepared are tabulated in Table 2. Most of the measurement items are designed to follow the NTF's model.<sup>6</sup> The model has 370 pressure taps, which consists of 325 taps on the main wings, 12 taps on the fuselage and 33 taps on the horizontal tails. The taps on the wings are located in 9 span-wise wing sections ( $\eta = 0.131, 0.201, 0.283, 0.397, 0.502, 0.603, 0.727, 0.846, \text{ and } 0.950$ ) as the same location of the NTF's model and 1 location at  $\eta = 0.312$  originally on the lower surface of the main wing. The pressures are led to the installed electronically scanned pressure sensor (ESP) modules by stainless tubes with the inner diameter of 0.8 mm. The ESP system used is the System 8400 of Pressure System Inc. The pressure taps of one wing section is basically apportioned to the left and right main wings to pack tubes, the left main wing holds upper surface pressure taps and the right main wing covers the lower surface, while the trench to install the pressure tubes are curved symmetrically to keep the bending characteristics of both wings to be same. Pressure tap arrangement images are illustrated in Fig. 5. The locations indicated by black texts were used for this campaign and other taps were not used because of ESP capability limitation.

The model was installed in the test section supported by the sting through the 6-component force balance. The balance specifications are listed in Table 3. The support sting was fabricated to simulate the original sting of the NTF while the test section of the JTWT is shorter and the aft-end of the sting shape was trimmed off to place the model in the proper location of the test section.

Static measurement consists of aerodynamic force, surface pressure distribution and main wing deformation measurement. The surface pressure distribution measurement includes wind tunnel wall surface pressure measurement for wall interference correction. The aerodynamic force measurement was performed using a 6-component force balance which is installed in the wind tunnel model.

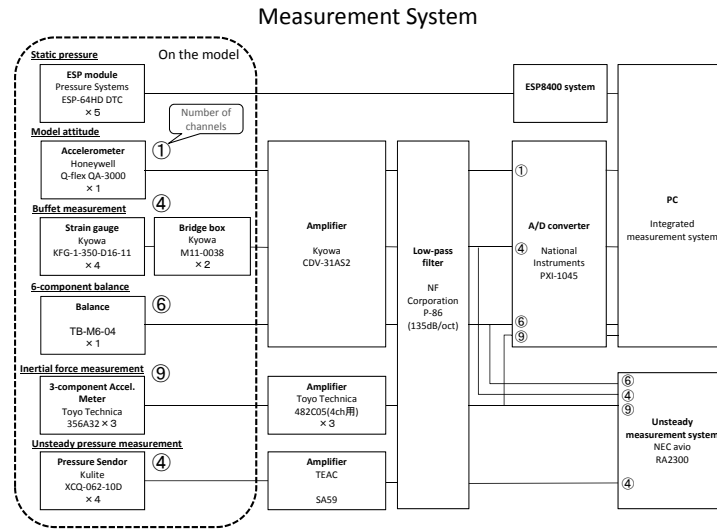


Figure 4. Block diagram of measurement system

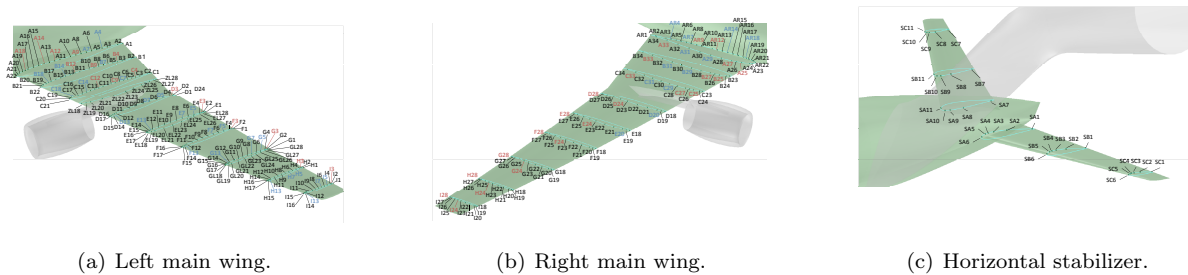


Figure 5. Pressure tap locations

Unsteady pressure measurement on the surface of the main wing and strain gauge measurement for main wing bending and torsion was also performed, while unsteady measurement are introduced by the other literature<sup>13</sup>

### II.C.2. Model Deformation

Wind tunnel model is deformed due to the dynamic pressure. Thus, the model deformation was measured in the test. The deformation of the model was considered to work mainly on the main wings. And, the model main wings were fabricated as symmetrical as possible to make the deformation of both of the main wing to be symmetric. The deformation of only the left main wing was, therefore, measured by an optical measurement method. The measurement system consists of three cameras of Allied Vision Technologies. One camera (29 Megapixel Prosilica GX6600) was looking down from the test section ceiling and two cameras (16 Megapixel GE4900) were looking through the windows on the side walls.

The measurement was performed by 3-D positioning of markers on the model surface. On the main wings, 60 markers were prepared for the measurement. The markers are located at 15, 55 and 95% chord length of 5 sections at  $\eta = 0.16575, 0.33995, 0.5526, 0.7862, 0.975$  on the upper surface of the main wings, and 30 markers are located on the body upper surface.

The measurement results at  $M_{pc} = 0.85$  are figured in Fig. 7.

Measurement objectives	Prepared equipment
Aerodynamic force	installed 6-component balance
Static pressures	325 taps on the main wing 33 taps on the horizontal stabilizer 12 taps on the body 5 taps on the support sting surface 10 taps on the left nacelle surface 5 total pressure through the left nacelle
Unsteady Pressure	3 taps on the upper surface of the left main wing 1 tap on the lower surface of the right main wing
Strain gauge	2 for each main wing bending 2 for each main wing torsion
Model shape deformation	30 markers on the model surface

**Table 2. Measurement devices on the model.**

Name	Range					
	$F_x$	$F_y$	$F_z$	$M_x$	$M_y$	$M_z$
TB-M6-04	670 N	4000 N	8000 N	226 N-m	565 N-m	226 N-m

**Table 3. Balance specifications**

## II.D. CFD Simulations

Pre-test CFD simulations were performed before the wind tunnel test campaign to make direct comparisons with wind tunnel data.

The TAS code,<sup>14</sup> which is based on a cell-vertex finite volume method, was used as the flow solver. Reynolds averaged Navier-Stokes equations were solved with the numerical flux computations employing Harten-Lax-van Leer-Einfeldt-Wada (HLLW) method.<sup>15</sup> For the time integration, the Lower/Upper Symmetric Gauss-Seidel (LU-SGS) implicit method<sup>16</sup> was used. The boundary layer model used was Spalart-Allmaras one-equation turbulence model<sup>17</sup> without the trip term for transition. To estimate anisotropic Reynolds stress tensor, Spalart's model was employed.<sup>18</sup>

The computational grid is in the configuration of wing/body/tail = 0° and including the sting shape close to the model (Fig. 8). The computation was performed at a freestream Mach number of 0.85 and the Reynolds number based on the reference chord length  $c_{ref}$  was set at  $Re_c = 5.0$ . The angles of attack were set at 0, 1, 2, 2.558 ( $C_L = 0.5$ ), 3, 4 and 5 degrees.

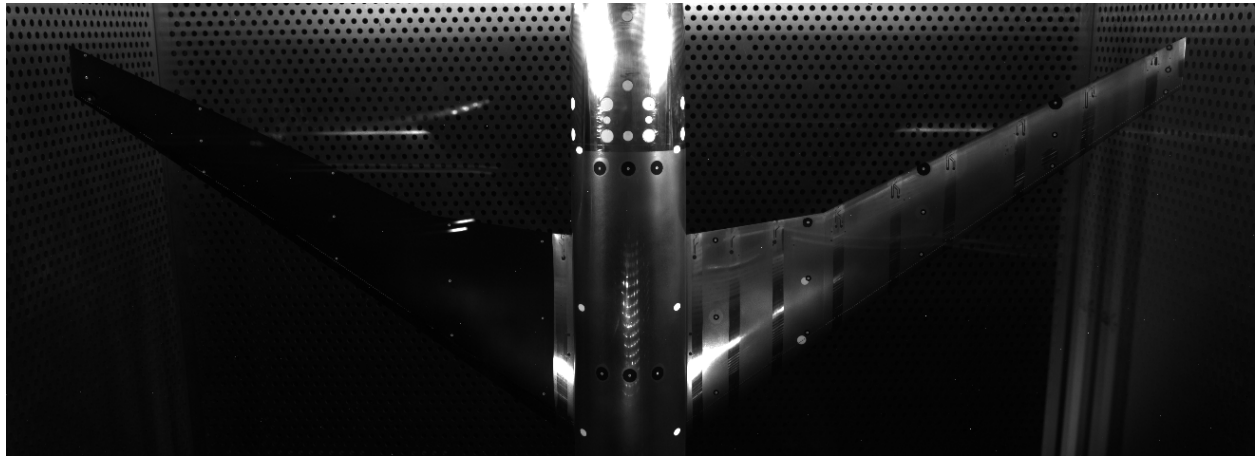
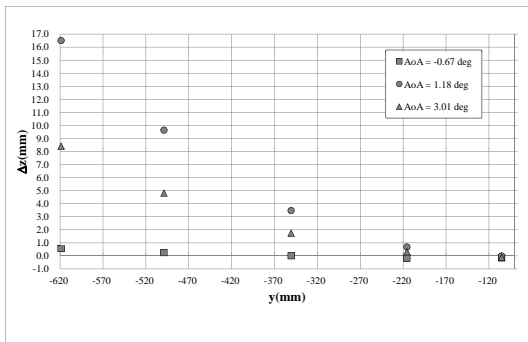
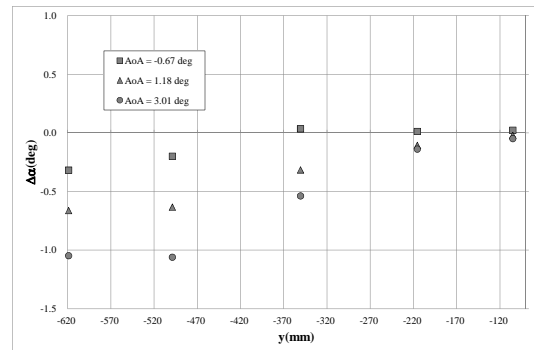


Figure 6. Image captured by a model deformation measurement camera.



(a)  $\Delta z$ .



(b)  $\Delta \alpha$ .

Figure 7. Deformation of the left main wing.

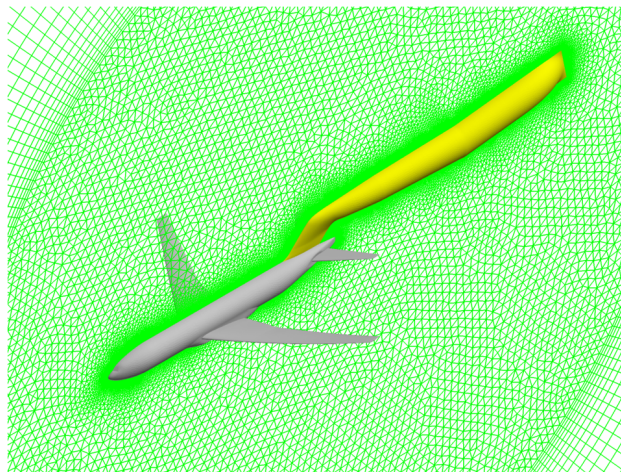


Figure 8. Symmetric plane cut out image of computational grid of pre-test CFD.

### III. Test Conditions

#### III.A. Wind Tunnel Test

The static measurement items are aerodynamic force and moment, pressure distribution on the model surface, model deformation and wind tunnel wall pressure distribution.

The Reynolds number was set at  $2.27 \times 10^6$ , and the total pressure ( $P_0$ ) was set at 120 kPa to achieve it. The Reynolds number was selected because of the total pressure limit of the wind tunnel. To force boundary layer around the wind tunnel model to be turbulent, trip dots are stuck on the main wings, the horizontal stabilizers and the nose of the body. The trip dots which have a diameter of 1.27 mm and spaced 2.54 mm were located at 10% of chord of the wings and 1.5% station of the body. The heights of the trip dots were optimized following Braslow and Knox<sup>19</sup> and they are tabulated in Table 4.

Part	Height [mm]
From the side of body to the yehudi break	0.089
From the yehudi break to the midwing	0.079
From the midwing to the wing tip	0.079
Horizontal stabilizers	0.079
Nose	0.064

Table 4. Height of trip dots

The horizontal stabilizers were attached and the deflection angle of them was fixed at 0 deg. The sideslip angle was fixed at 0 deg. Mach number calculated using plenum chamber static pressure was set at  $M_{pc} = 0.7, 0.83, 0.85, 0.86$  and  $0.87$ . However, the results only at the  $M_{pc} = 0.85$  is discussed in this article. The pitch angle of the model support system was varied approximately from -2 to 5 deg.

## IV. Data Reduction and correction

### IV.A. Classical corrections

At first, the flow angle correction was performed using upright pitch run data. Then, Mach number correction based on the difference between the test section static pressure measured by a static pressure probe in the empty wind tunnel calibration test and the buoyancy correction using the data of long static pressure probe aligned in the center of the test section also in the empty calibration test were applied. After that, wall interference correction was applied. The details of the wall interference corrections are stated in another paper by the authors.<sup>20</sup>

The Reynolds number of the JTWT was set at relatively lower value ( $2.27 \times 10^6$ ) than that of the NTF and CFD tests ( $5.0 \times 10^6$ ). To compare with those results, Reynolds number correction using skin friction coefficient of flat plate was applied. The correction was computed as the difference between the estimated parasite-drag at  $Re$  of the JTWT wind tunnel test and that of the NTF and CFD tests. The parasite-drag was built up using the following equation as a sum of friction drag of each component:<sup>21</sup>

$$C_{D0} = \frac{\Sigma (C_f \cdot FF \cdot Q \cdot S_{wet})}{S_{ref}} \quad (1)$$

where  $C_f$  is friction drag of each component,  $FF$  is the ‘‘form factor’’ which estimates the pressure drag due to viscous separation and  $Q$  is the interference effect factor. Raymer<sup>21</sup> states that the fuselage has a negligible interference factor ( $Q = 1.0$ ) in most cases and the interference will be negligible for a well-filletted low wing. In this article, all the  $Q$  were, therefore, set as 1.0. Fully turbulent flat plate skin friction coefficient was computed by:

$$C_f = \frac{0.455}{(\log_{10} Re)^{2.58} (1 + 0.144M^2)^{0.65}}. \quad (2)$$

And, the form factors of the wing and the tail were computed by:

$$FF = \left\{ 1 + \frac{0.6}{(x/c)_m} \left( \frac{t}{c} \right)^4 \right\} \left\{ 1.34M^{0.18} (\cos \Lambda_m)^{0.28} \right\}. \quad (3)$$

In Eq. 3, the term ‘‘ $(x/c)_m$ ’’ is the chordwise location of the airfoil maximum thickness point,  $t$  is the thickness of the wing,  $c$  is the chord length and  $\Lambda_m$  refers to the sweep of the maximum-thickness line. The fuselage form factor was computed by:

$$FF = \left( 1 + \frac{60}{f^3} + \frac{f}{400} \right) \quad (4)$$

where

$$f = \frac{l}{d} = \frac{l}{(4/\pi)A_{max}}.$$

$l$  is length of the body,  $d$  is a reference diameter of the body, and  $A_{max}$  is the maximum cross sectional area of the body.

Then, the correction due to Reynolds number difference was calculated as:

$$\Delta C_{D0} = C_{A0}|_{Re=5 \times 10^6} - C_{D0}|_{Re=2.27 \times 10^6}. \quad (5)$$

### IV.B. Data Normalization

To make a fair comparison among various data sources, the outputs should be normalized to a designated conditions, i.e., the design shape flying at design point in free-air. Flow conditions of wind tunnel test results are corrected by conventional wind tunnel wall corrections. However, the wind tunnel model profiles are usually deformed by dynamic pressure. The deformation effects, which is mainly exerted on the main wings, should be corrected.

A model deformation measurement result of the CRM in the JTWT are shown in Fig. 7. It shows that the ‘‘real’’ angle of attack at the wing tip is twisted more than 1 deg down from the model angle of attack in the case of the model angle of attack is 3 degree. This means fair comparisons cannot be achieved without corrections. The angle of attack at each wing section should be aligned in the normalized data.

#### IV.B.1. Pressure Distribution

Pressure distribution on each wing section should be corrected by replacing data at the angle of attack which was calculated subtracting angle of attack deformation in Fig. 7(b). Because the wing deformation data was acquired on dispersed wing sections, the data was interpolated to acquire change in twist at each section. Then, the change in twist was subtracted at each wing section from the model angle of attack which was output as the model attitude. Each pressure distribution was replaced with the data which was computed by interpolation at the corrected angle of attack. Thus, the pressure data was mostly replaced with the data at the higher model angle of attack.

Both of the uncorrected and the corrected pressure distributions are shown from Fig. 10–18. In the figures, the pressure distributions from JAXA’s wind tunnel test at the Reynolds number of  $2.2 \times 10^6$ , JAXA’s CFD test at the Reynolds number of  $5 \times 10^6$  and the NASA NTF’s wind tunnel test at the Reynolds number of  $5 \times 10^6$  are shown. Data at three angles of attack of 0, 2 and 4 are compared. Because the wind tunnel data were not acquired at those angles of attack, the data were interpolated to the angles. Model deformation data of JAXA’s wind tunnel test come from the data explained above (Section II.C.2). All the NASA’s data was acquired from the NASA CRM web site.<sup>22</sup> Especially at the wing sections which is close to the wing tip, such as Section I (Fig. 18, deformation correction effectiveness is remarkable. Dynamic pressure generally twist the main wing harder than the original shape, and the actual angle of attack at each wing section is lowered. Thus, the negative pressure distributions appear lower than that of CFD data. However, with applying wing deformation corrections, the wind tunnel data go closer to the CFD data.

#### IV.B.2. Balance Output

The balance output is also affected by model deformation because the change in twist distribution changes pressure distribution so that the net force varies from that of the designed shape. To make a comparison among data from various data sources, normalization of net aerodynamic forces is desirable. To accomplish this, surface pressure data was used again. As the results of numerical integration of surface pressures at each wing section, 2-dimensional lift ( $c_l$ ) and drag ( $c_d$ ) at each section can be approximately computed:

$$c_n = \sum_{i=1}^N (x(i+1) - x(i)) \frac{c_p(i+1) + c_p(i)}{2} + (x(1) - x(N)) \frac{c_p(1) + c_p(N)}{2} \quad (6)$$

$$c_a = - \sum_{i=1}^N (z(i+1) - z(i)) \frac{c_p(i+1) + c_p(i)}{2} - (z(1) - z(N)) \frac{c_p(1) + c_p(N)}{2} \quad (7)$$

$$c_l = c_n \cos \alpha - c_a \sin \alpha, \quad (8)$$

$$c_d = c_a \cos \alpha + c_n \sin \alpha. \quad (9)$$

Span-wise distributions of  $c_l \times c$  (lift distribution) are shown in Fig. 19.

They can be replaced by the data at the proper angles of attack which was acquired by subtracting the change in twist angles interpolated at the wing sections with the same way to compute section pressure distribution in Sec. IV.B.1. Integrating those section force coefficients in span-wise direction eventually gives the forces which is to be exerted if the shape of the wind tunnel model were not deformed due to the dynamic pressure.

$$C_{L\text{wing}} = \sum_{j=1}^M (c_l(j)c\Delta b), \quad (10)$$

$$C_{D\text{wing}} = \sum_{j=1}^M (c_d(j)c\Delta b). \quad (11)$$

Without pressure replacement, the integral brings the force actually exerts under the conditions of deformation due to dynamic pressure. The difference of those two integrals could be expected to give the correction of force coefficients.

$$\Delta C_{L\text{wing deformation}} = C_{L\text{wing}}|_{\text{normalized}} - C_{L\text{wing}}|_{\text{deformed}}, \quad (12)$$

$$\Delta C_{D\text{wing deformation}} = C_{D\text{wing}}|_{\text{normalized}} - C_{D\text{wing}}|_{\text{deformed}} \quad (13)$$

Finally, the  $C_L$  and the  $C_D$  were corrected as follow:

$$C_{L\text{corrected}} = C_L + \Delta C_{L\text{wing deformation}}, \quad (14)$$

$$C_{D\text{corrected}} = C_D + \Delta C_{D0} + \Delta C_{D\text{wing deformation}} \quad (15)$$

The uncorrected and corrected lift and drag are shown in Fig. 20–22.

## V. Analysis

### V.A. Pressure Distribution

#### V.A.1. Wing Deformation Correction Effect

As stated in Section IV.B.1, the pressure distribution at the wing section where the static pressure ports are located are shown in Fig. 10–18. Without wing deformation correction, negative pressure levels on the upper surface of the wind tunnel tests are largely different from estimated pressure level of CFD, especially around the wing tip where the changes in twist are large. However, when the wing deformation was corrected, those discrepancy decrease remarkably. The differences between the data of the JTWT and the NTF also agree fairly well while the Reynolds number of those tests are different.

#### V.A.2. Shock Location

The shock locations estimated by CFD were generally more downstream than those of wind tunnel tests, and it is noticeable especially at the mid-wing (Fig. 14(b) and 15(b)). When the angle of attack is 4 degree, the shape of the pressure profile are common but the shock location is downstream in the case of CFD. On the other hand, in the case of the angle of attack is 2 degree, the CFD results show that there are two stages of shocks, while the pressure distribution of wind tunnel tests show the secondary shock to be weaker.

#### V.A.3. Lift Distribution

After the deformation correction, integrated lift distributions were compared with each other (Fig. 19(b)). Noticeable differences between the wind tunnel distributions and the CFD is seen around  $\eta = 0.5$  to 0.6 at the angle of attack of 4 degree. This should come from the large difference of the shock location which is noticed in Section V.A.2.

With CFD analyses, it is predicted separation starts around the area. Thus, improvement of such kind of shock induced separation prediction would be expected to correspond to the improvement of lift distribution and net aerodynamic force estimation.

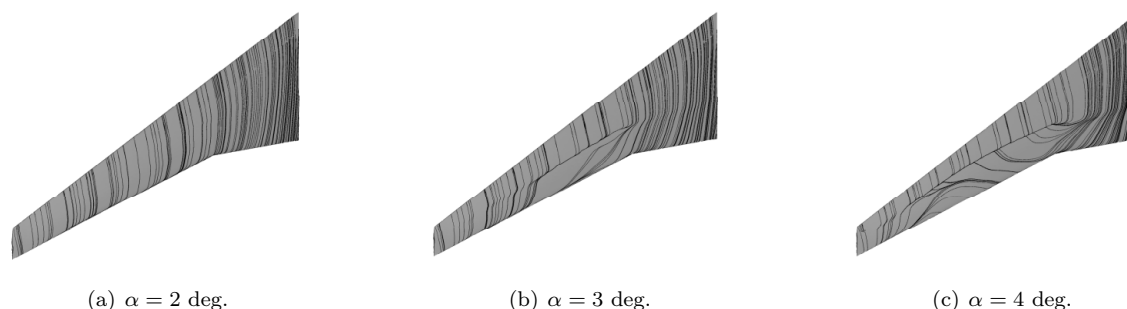


Figure 9. Streamlines on the upper surface computed by CFD.

### V.B. Force Coefficient

#### V.B.1. $C_L$ vs $\alpha$

The wing deformation correction is substantially effective on the lift characteristics (Fig. 20(c)). This result is coherent with the result stated by Rivers *et al*<sup>11</sup> which a CFD estimation performed with the computational grid with deformed wings under the wind tunnel test circumstances.

#### V.B.2. $C_D$ vs $\alpha$

At first, the classical Reynolds number correction works well and the corrected drag curve of the JTWT test agrees very well with the curve of the NTF as shown in Fig. 21(b). Although the wing deformation correction works well for the lift characteristics, the correction on the drag characteristics enlarged the

discrepancy between the results of the JTWT and the NTF while average of them moved closer to the CFD curve (Fig. 21(c)).

### V.B.3. Drag Polar

In the case of drag polar, agreement among the data of the JTWT, the NTF and the CFD seems to be the closest only with the Reynolds number correction. However, the agreement between the wind tunnel test results is the best when the wing deformation correction is applied, except the range of  $C_L$  from 0.2 to 0.5.

## VI. Summary

A set of wind tunnel test of the 80% scaled NASA Common Research Model was performed at the 2m  $\times$  2m transonic wind tunnel (JTWT) of Japan Aerospace Exploration Agency. The results was compared with the results of the NTF and the CFD estimation which employed the grid simulating the existence of the support sting.

Besides the basic classical wind tunnel corrections, a Reynolds number correction based on the turbulent friction estimation and the wing deformation correction were applied to the wind tunnel data for normalization to make a comparison among the data from different sources.

The pressure distribution at each wing section, the span-wise lift distribution and the net lift and drag characteristics were examined.

Thus, the following conclusions were acquired for pressure distributions:

- The wing deformation correction for the wing sections improved the agreement among the pressure distributions from the JTWT, the NTF and the CFD.
- The shock location predicted by the CFD is generally at more downstream than the wind tunnel results.

Then, the span-wise lift distributions were acquired by integrating the pressure distribution on the main wings, and:

- The noticeable discrepancy between the wind tunnel data and the CFD is observed in the wing deformation corrected case of the angle of attack of 4 degree around the mid-wing.
- The discrepancy was assumed to be caused by shock induced separation difference between the test and the CFD.

Eventually, the conclusions for the net aerodynamic lift and drag were acquired as follows:

- The wing deformation correction is remarkably effective for the lift coefficient characteristics.
- The Reynolds number correction based on the turbulent friction estimation successfully brings a good agreement between the data of the JTWT at the Reynolds number of  $2.27 \times 10^6$  and that of the NTF at  $5 \times 10^6$ .
- The wing deformation correction enlarges the discrepancy between the wind tunnel results while the mean value of them are made closer to the CFD estimation.
- The wing deformation correction achieves the agreement of the drag polar curves between the wind tunnel test results except for the range of  $C_L$  from 0.2 to 0.5 while the discrepancy between the wind tunnel test and the CFD is enlarged.

The corrections applied in this article are significantly effective for the study of pressure distribution and lift. On the other hand, it is not enough for examining drag. Nevertheless, data normalization techniques are crucial to make fair comparisons among the data from various sources. Therefore, improvement of the techniques would be anticipated.

## Acknowledgments

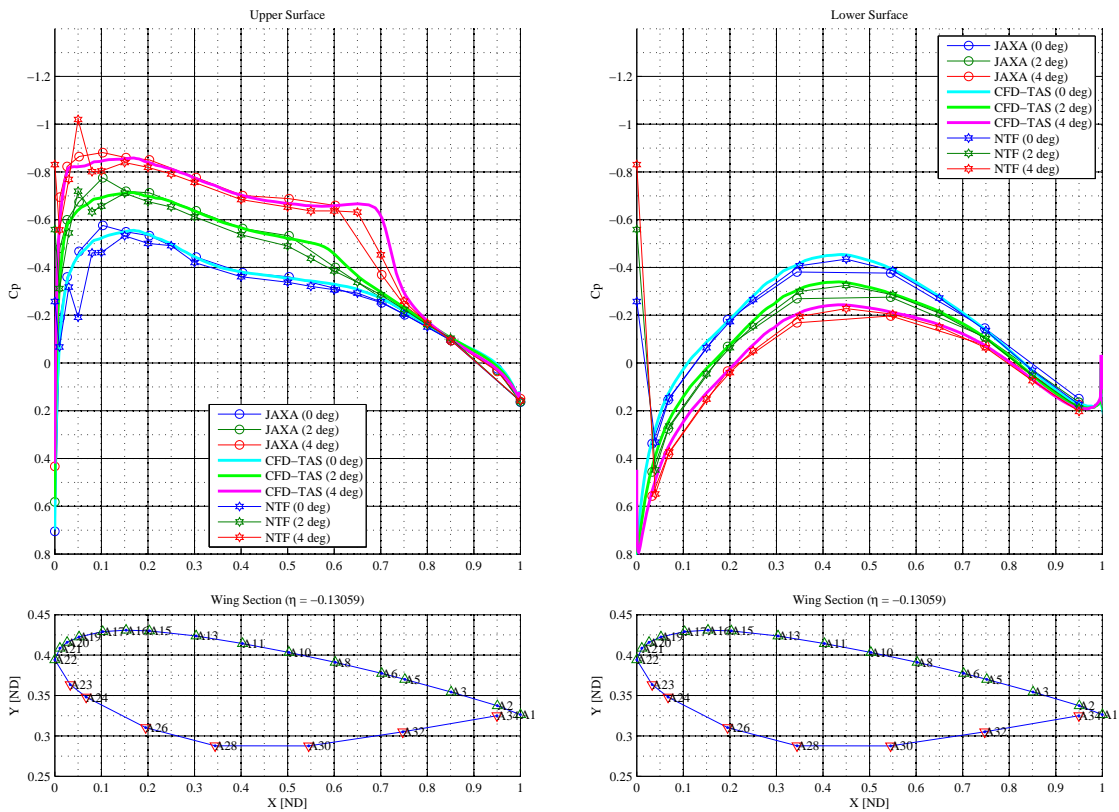
The authors would like to gratefully acknowledge Ms. Melissa B. Rivers of NASA Langley Research Center for providing essential advices to fabricate a copy of the NASA CRM. She and the staffs of the National Transonic Facility of NASA kindly gave the authors various information about the NASA CRM. The authors also would like to appreciate Dr. John C. Vassberg for cleaning up the surface data of the nose part of the CRM. The authors would also like to appreciate Mr. Kentaro Tanaka and Mr. Tohru Hirai for their support mainly for computational operations and Dr. Kanako Yasue and Dr. Kentaro Imagawa for their long term efforts of output definitions of JAXA's CRM test campaigns.

## References

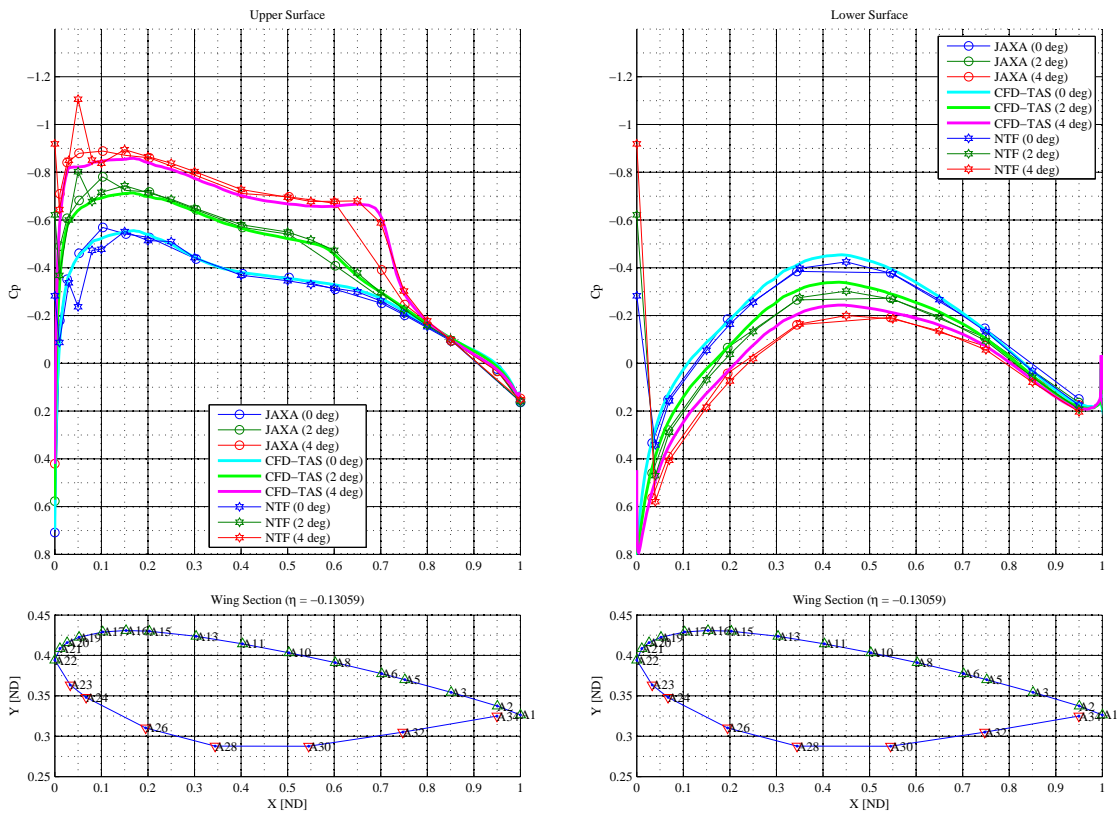
- <sup>1</sup>Levy, D., Wahls, R., Zickuhr, T., Vassberg, J., Agrawal, S., Pirzadeh, S., and Hensch, M., "Summary of Data from the First AIAA CFD Drag Prediction Workshop," AIAA Paper AIAA 2002-841, 40th AIAA Aerospace Sciences Meeting and Exhibit, Jan. 2002.
- <sup>2</sup>Laffin, K., Brodersen, O., Rakowitz, M., Vassberg, J., Wahls, R., Morrison, J., Tinoco, E., and Godard, J.-L., "Summary of Data from the Second AIAA CFD Drag Prediction Workshop," AIAA Paper 2004-555, 42nd AIAA Aerospace Sciences Meeting and Exhibit, Reno, NV, Jan. 2004.
- <sup>3</sup>Vassberg, J., Tinoco, E., Mani, M., Brodersen, O., Eisfeld, B., Wahls, R., Morrison, J., Zickuhr, T., Laffin, K., and Mavriplis, D., "Summary of the Third AIAA CFD Drag Prediction Workshop," AIAA Paper 2007-260, 45th AIAA Aerospace Sciences Meeting and Exhibit, Jan 2007.
- <sup>4</sup>Vassberg, J., Tinoco, E., Mani, M., Rider, B., Zickuhr, T., Levy, D., Brodersen, O., Eisfeld, B., Crippa, S., Wahls, R., Morrison, J., Mavriplis, D., and Murayama, M., "Summary of the Fourth AIAA CFD Drag Prediction Workshop," AIAA Paper 2010-4547, 28th AIAA Applied Aerodynamics Conference, Jan 2010.
- <sup>5</sup>John C. Vassberg, Mark A. DeHaan, S. M. R. and Wahls, R. A., "Development of a Common Research Model for Applied CFD Validation Studies," AIAA Paper 2008-6919, Aug. 2008.
- <sup>6</sup>Rivers, M. B. and Dittberner, A., "Experimental Investigations of the NASA Common Research Model in the NASA Langley National Transonic Facility and NASA Ames 11-Ft Transonic Wind Tunnel," AIAA Paper 2011-1126, Jan. 2011.
- <sup>7</sup>Blakrishna, S. and Acheson, M. J., AIAA Paper 2011-1127, 49th AIAA Aerospace Sciences Meeting including the New Horizons Forum and Aerospace Exposition, Orlando, FL, Jan.
- <sup>8</sup>Bell, J. H., "Pressure-Sensitive Paint Measurements on the NASA Common Research Model in the NASA 11-ft Transonic Wind Tunnel," AIAA Paper 2011-1128, 49th AIAA Aerospace Sciences Meeting including the New Horizons Forum and Aerospace Exposition, Orlando, FL, Jan. 2011.
- <sup>9</sup>Zilliac, G. G., Pulliam, T. H., Rivers, M. B., Zerr, J., Delgado, M., Halcomb, N., and Lee, H., "A Comparison of the Measured and Computed Skin Friction Distribution on the Common Research Model," AIAA Paper 2011-1129, 49th AIAA Aerospace Sciences Meeting including the New Horizons Forum and Aerospace Exposition, Orlando, FL, Jan.
- <sup>10</sup>Rivers, M. B. and Hunter, C. A., "Support System Effects on the NASA Common Research Model," AIAA Paper 2012-0707, 50th AIAA Aerospace Sciences Meeting including the New Horizons Forum and Aerospace Exposition, Nashville, TN, Jan. 2012.
- <sup>11</sup>Rivers, M. B., Hunter, C. A., and Campbell, R. L., "Further Investigation of the Support System Effects and Wing Twist on the NASA Common Research Model," AIAA Paper 2012-3209, 30th AIAA Applied Aerodynamics Conference, New Orleans, LO, June 2012.
- <sup>12</sup>Yamamoto, K., Tanaka, K., and Murayama, M., "Comparison Study of Drag Prediction for the 4th CFD Drag Prediction Workshop using Structured and Unstructured Mesh Methods," AIAA Paper 2010-4222, 28th AIAA Applied Aerodynamics Conference, June 2010.
- <sup>13</sup>Koga, S., Kohzai, M., Ueno, M., Nakakita, K., and Sudani, N., "Analysis of NASA Common Research Model Dynamic Data in JAXA Wind Tunnel Tests," Aiaa paper, Jan. 2013.
- <sup>14</sup>Nakahashi, K., Ito, Y., and Togashi, F., "Some Challenges of Realistic Flow Simulations by Unstructured Grid CFD," *International Journal for Numerical Methods in Fluids*, Vol. 43, No. 6-7, Oct 2003, pp. 769-783.
- <sup>15</sup>Obayashi, S. and Guruswamy, G., "Convergence Acceleration of an Aeroelastic Navier-Stokes Solver," *AIAA Journal*, , No. 6, 1995, pp. 1134-1141.
- <sup>16</sup>Sharov, D. and Nakahashi, K., "Reordering of Hybrid Unstructured Grids for Lower-Upper Symmetric Gauss-Seidel Computations," *AIAA Journal*, , No. 3, 1998, pp. 484-486.
- <sup>17</sup>Spalart, P. and Allmaras, S., "A One-Equation Turbulence Model for Aerodynamic Flows," Tech. Rep. AIAA 92-0439, 30th Aerospace Sciences Meeting and Exhibit, Reno, NV, Jan 6-9 1992.
- <sup>18</sup>Spalart, P., "Strategies for turbulence modelling and simulations," *International Journal of Heat and Fluid Flow*, Vol. 21, 2000, pp. 252-263.
- <sup>19</sup>Braslow, A. L. and Knox, E. C., "Simplified Method for Determination of Critical Height of Distributed Roughness Particles for Boundary-Layer Transition at Mach Numbers from 0 to 5," NACA Technocal Note 4363, Sept. 1958.
- <sup>20</sup>Kohzai, M., Ueno, M., Koga, S., and Sudani, N., "Wall Interference Corrections of a NASA Common Research Model in JAXA Wind Tunnel Tests," Aiaa paper, Jan. 2013.
- <sup>21</sup>Raymer, D. P., *Aircraft design: A conceptual approach*, AIAA education series, American Institute of Aeronautics and Astronautics, Reston, Va., 3rd ed., 1999.
- <sup>22</sup>NASA, Langley Research Center, "Common Research Model," <http://commonresearchmodel.larc.nasa.gov/>.

## A. Data Figures

### A.A. Pressure Distribution on Each Wing Section

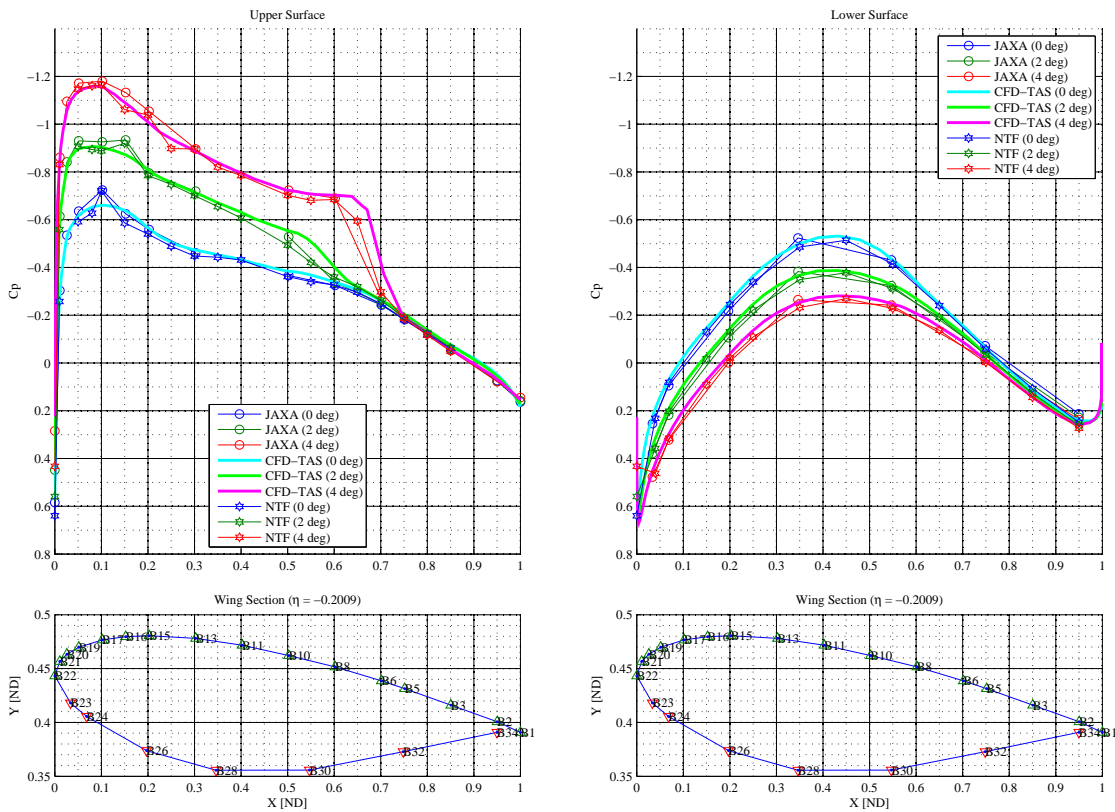


(a) Without wing deformation correction.

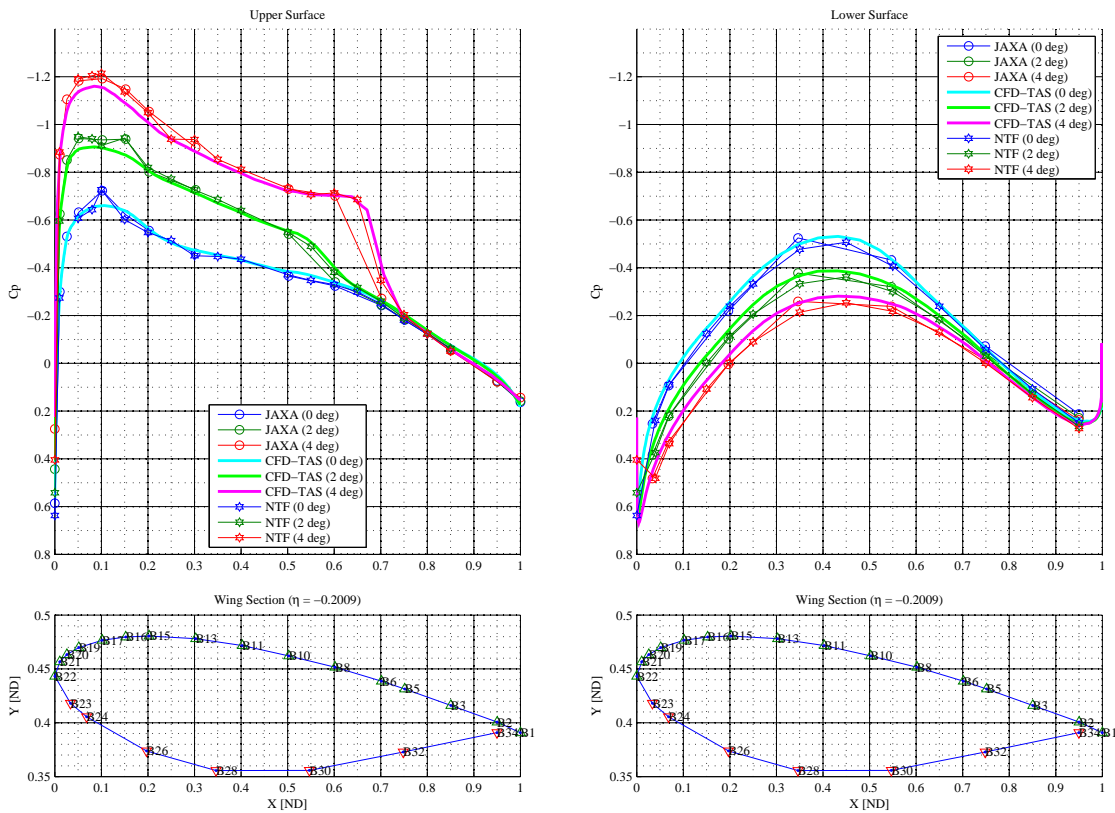


(b) With wing deformation correction.

**Figure 10. Pressure distribution at Section A.**

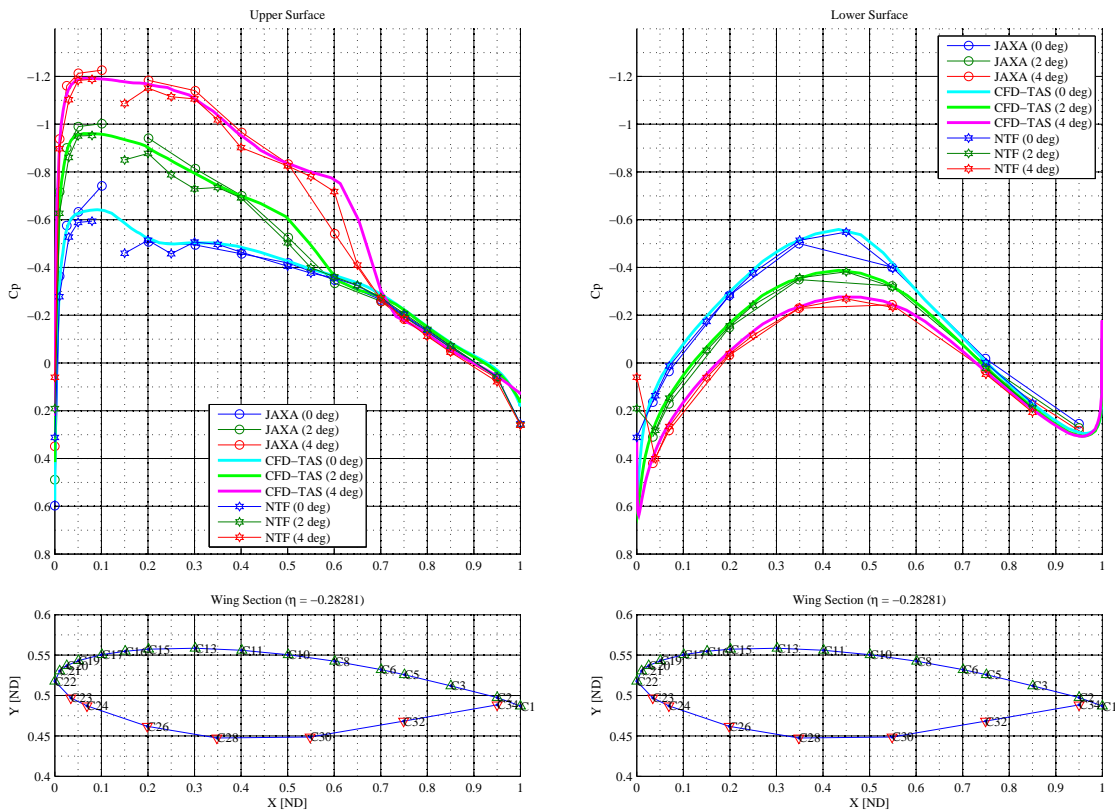


(a) Without wing deformation correction.

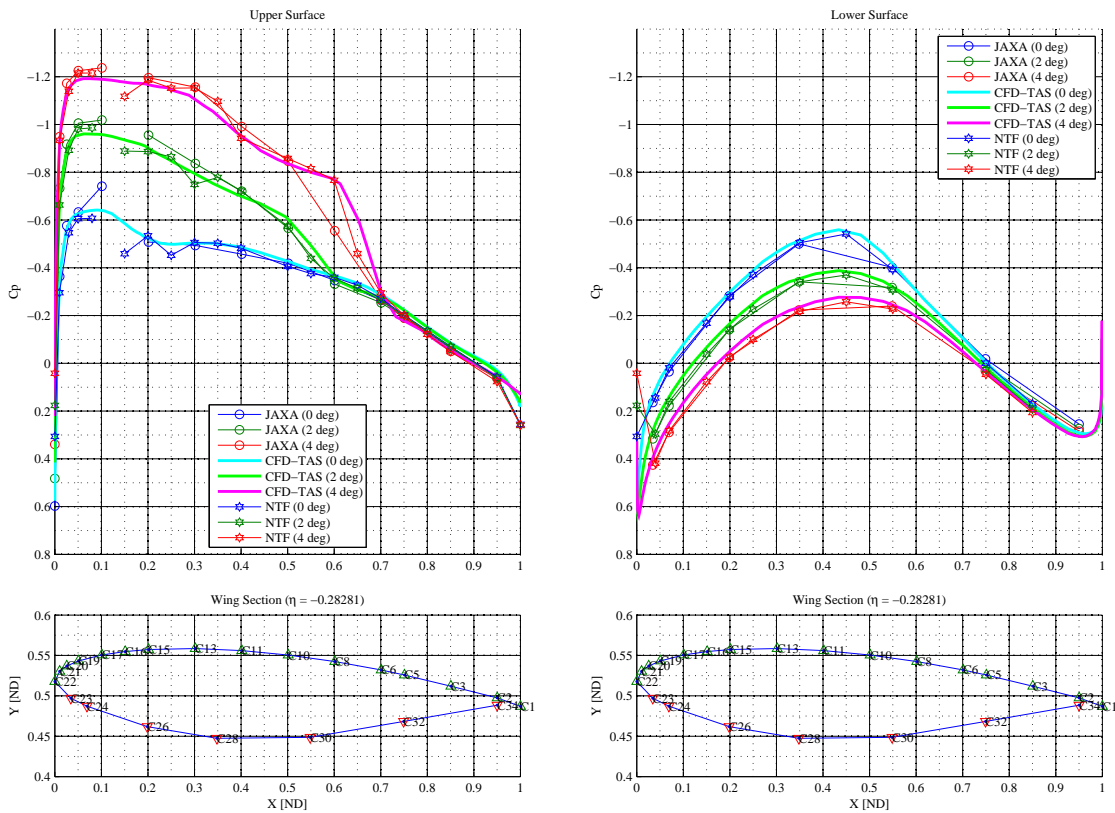


(b) With wing deformation correction.

**Figure 11. Pressure distribution at Section B.**

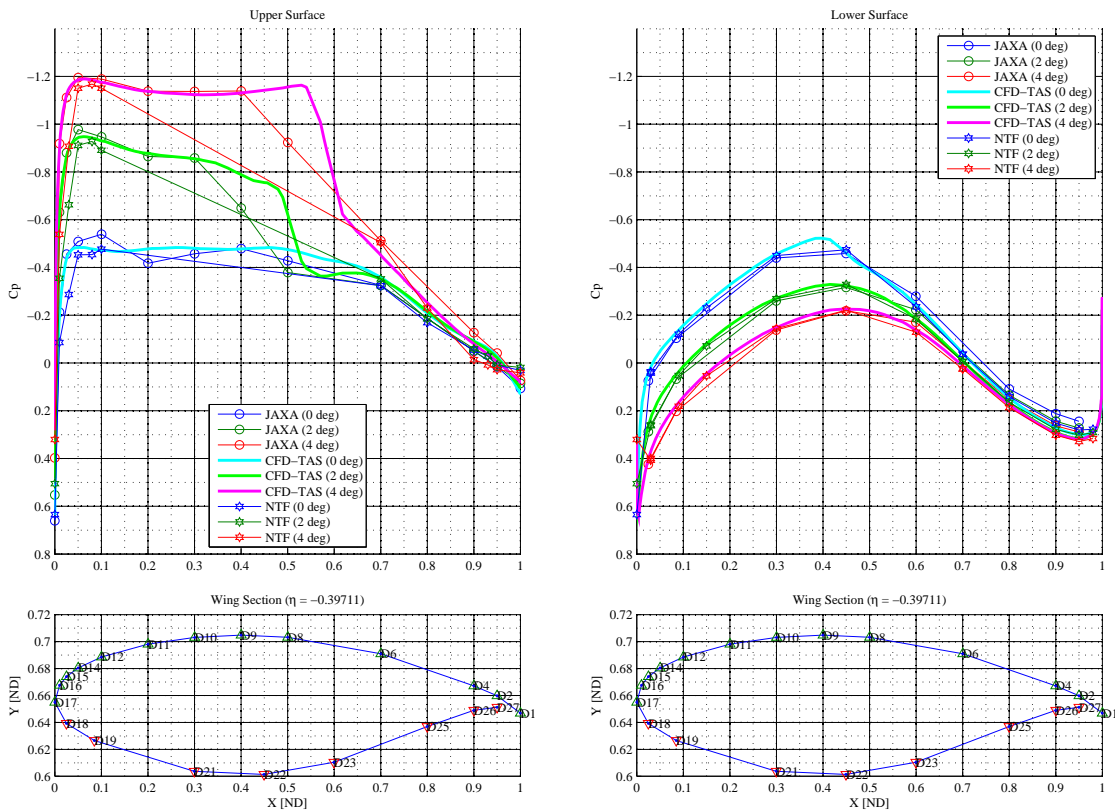


(a) Without wing deformation correction.

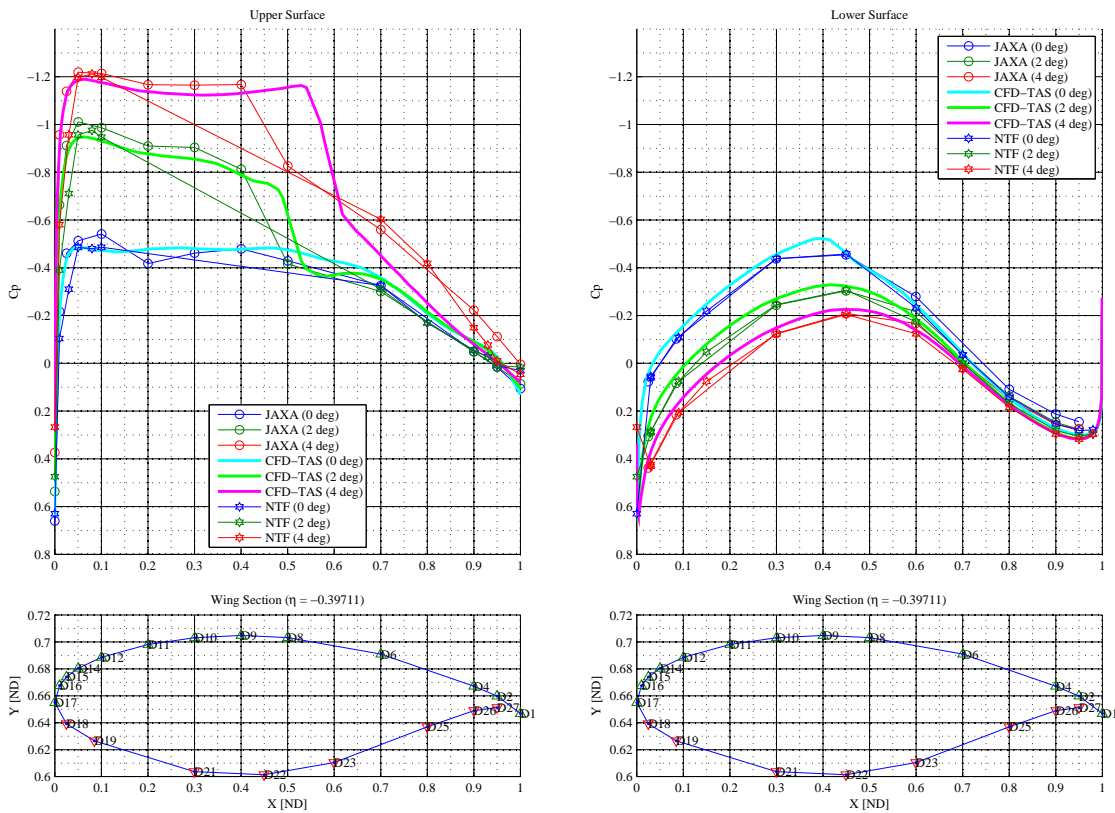


(b) With wing deformation correction.

Figure 12. Pressure distribution at Section C.

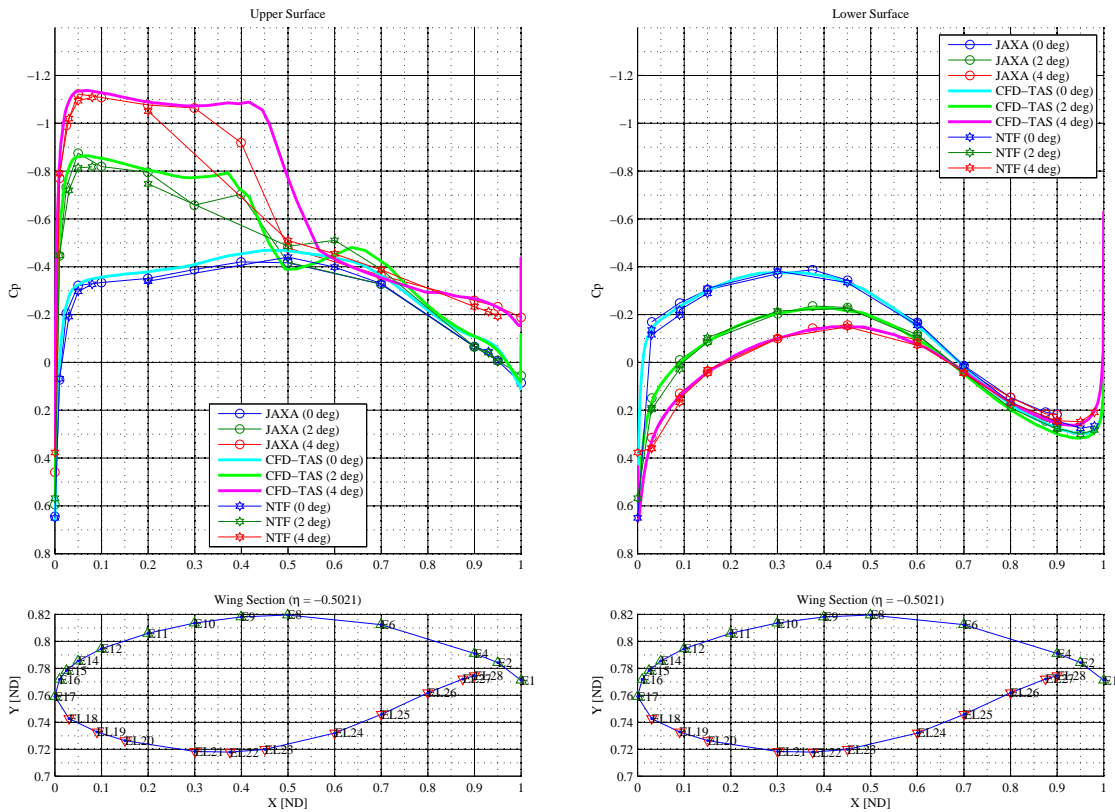


(a) Without wing deformation correction.

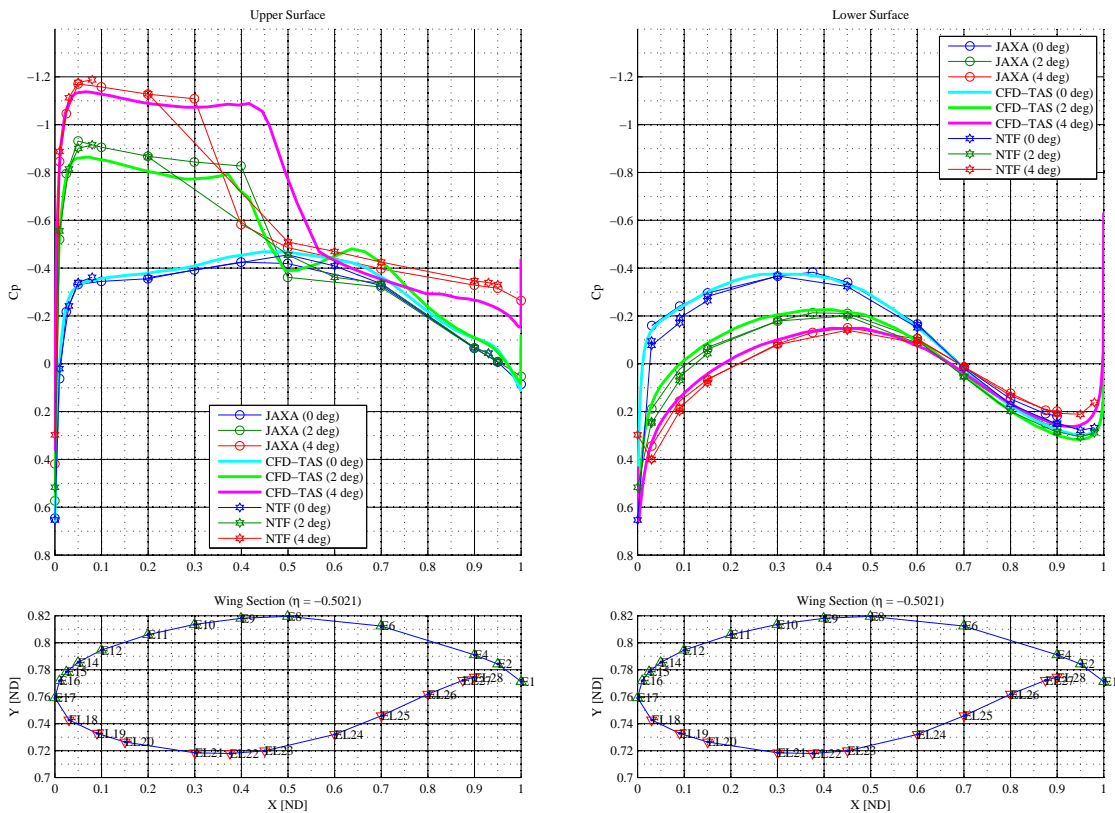


(b) With wing deformation correction.

**Figure 13. Pressure distribution at Section D.**

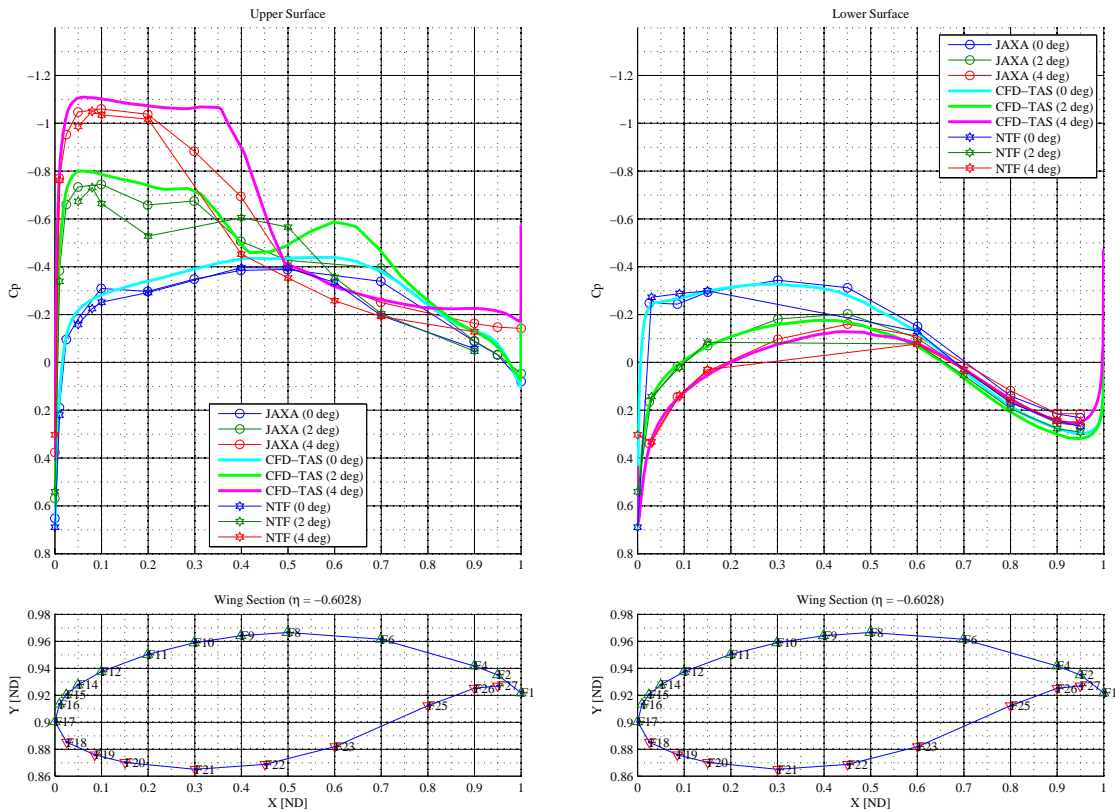


(a) Without wing deformation correction.

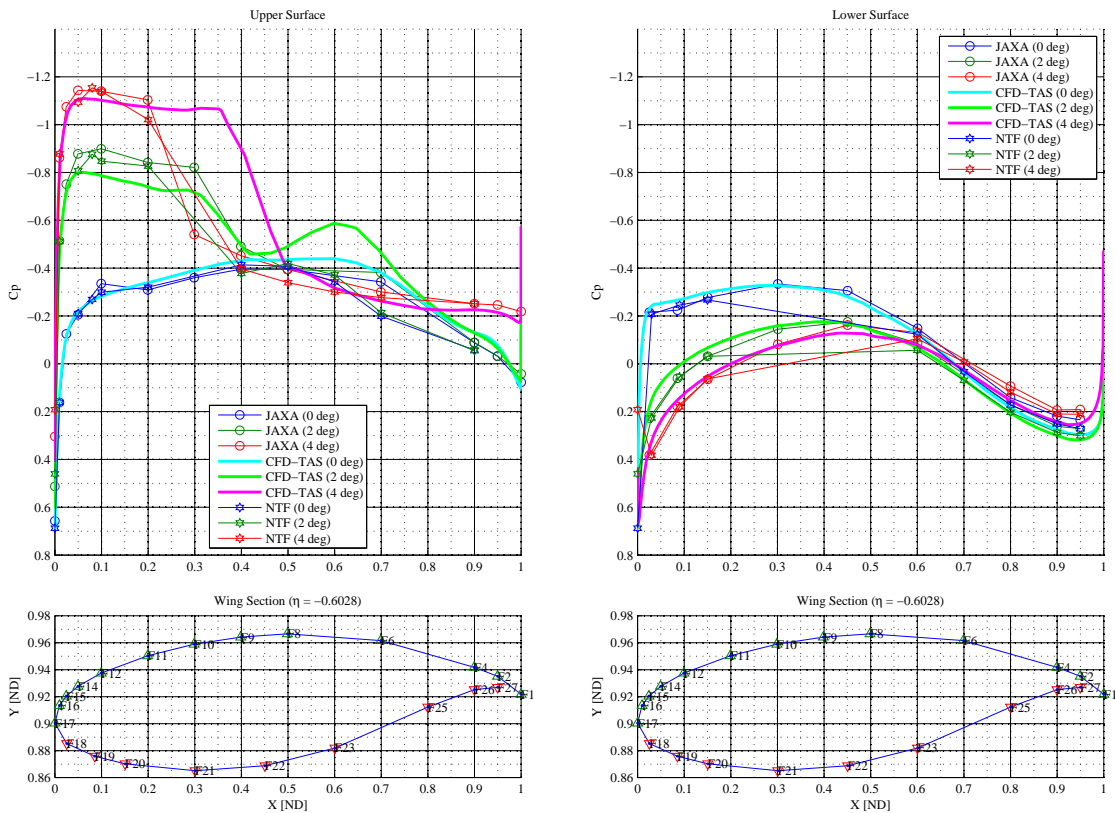


(b) With wing deformation correction.

Figure 14. Pressure distribution at Section E.

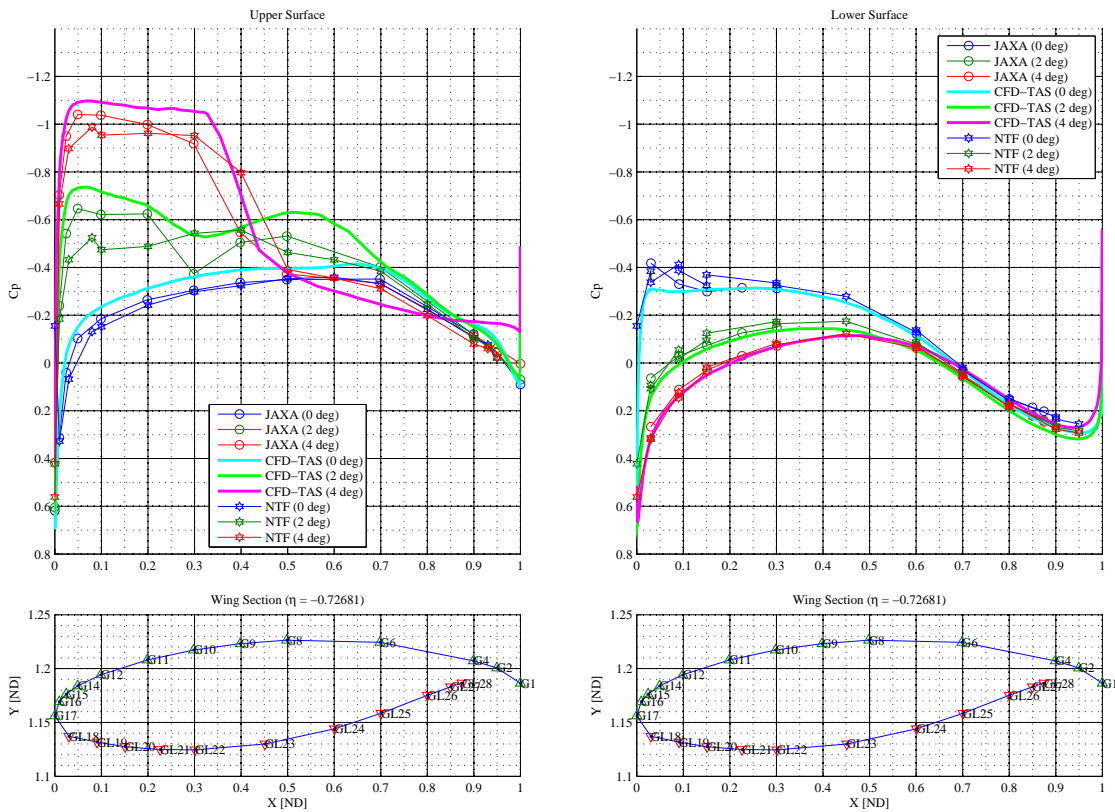


(a) Without wing deformation correction.

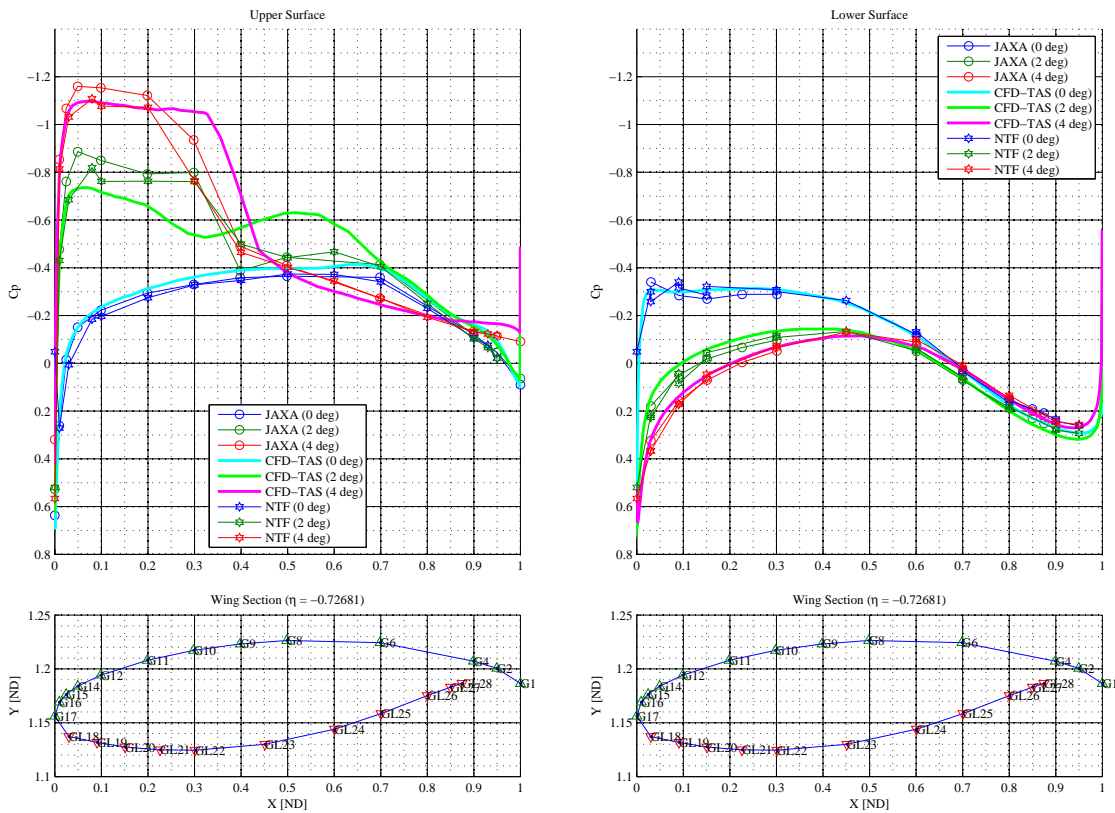


(b) With wing deformation correction.

Figure 15. Pressure distribution at Section F.

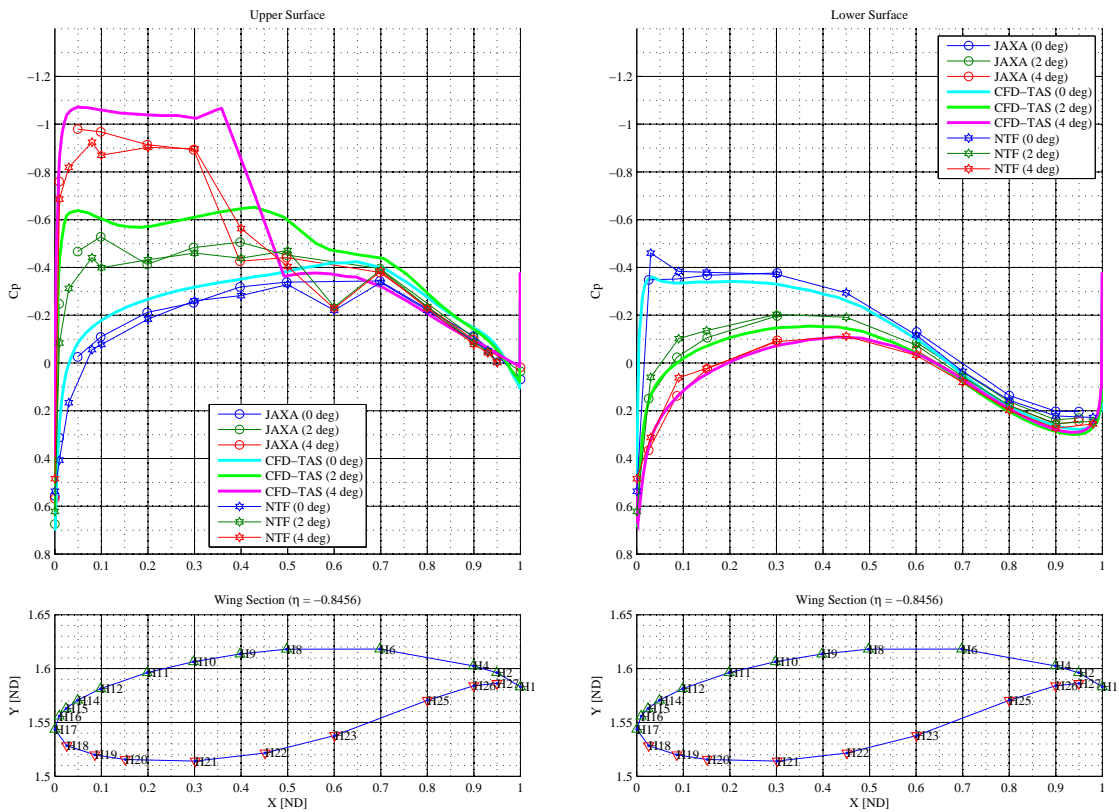


(a) Without wing deformation correction.

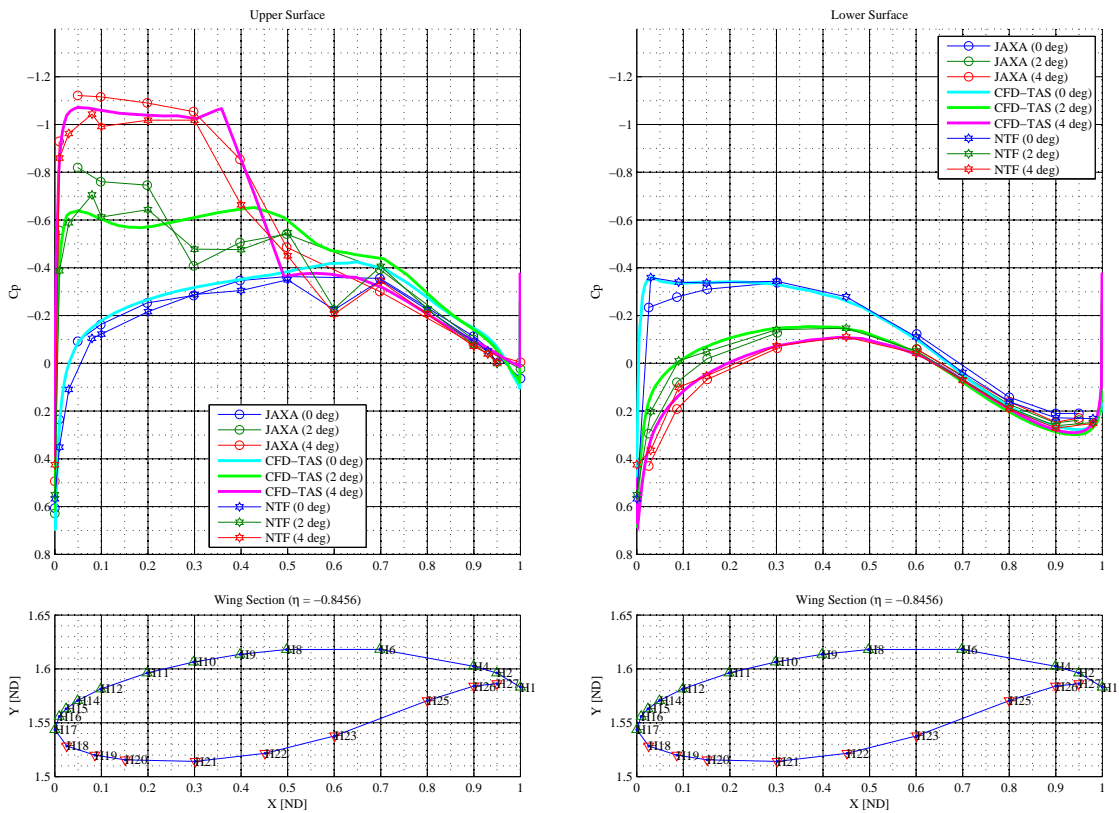


(b) With wing deformation correction.

Figure 16. Pressure distribution at Section G.

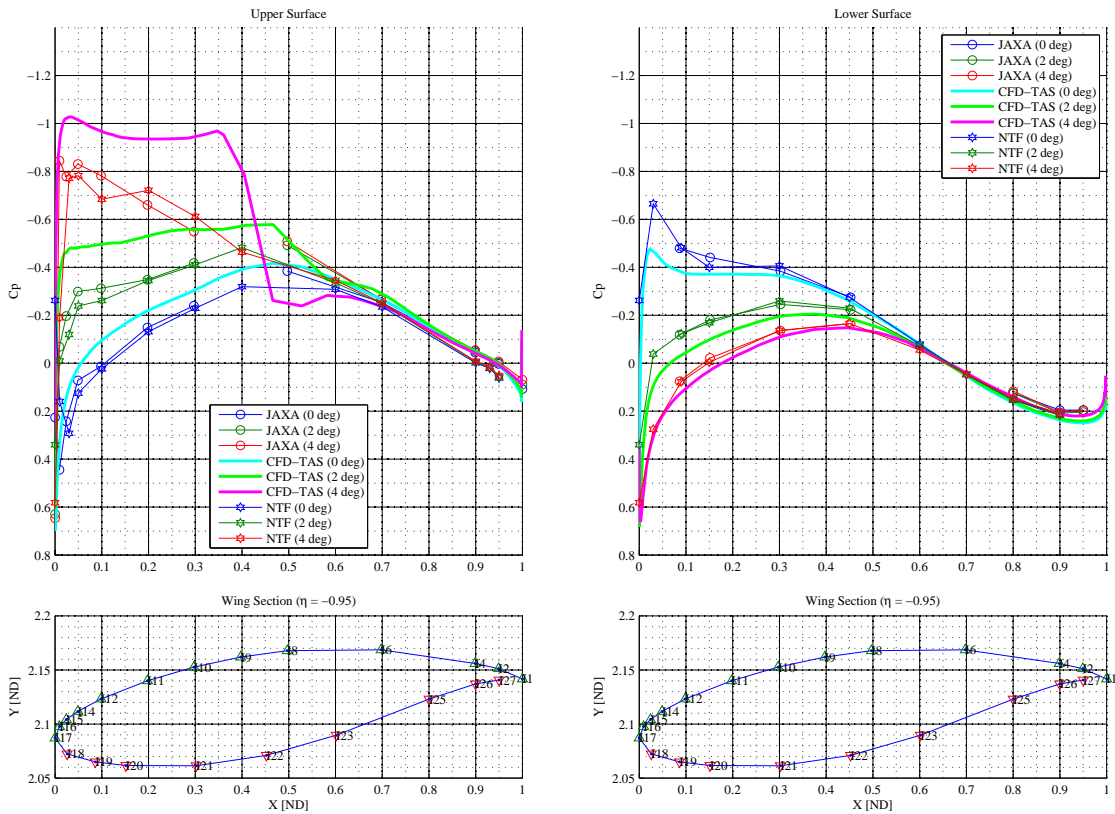


(a) Without wing deformation correction.

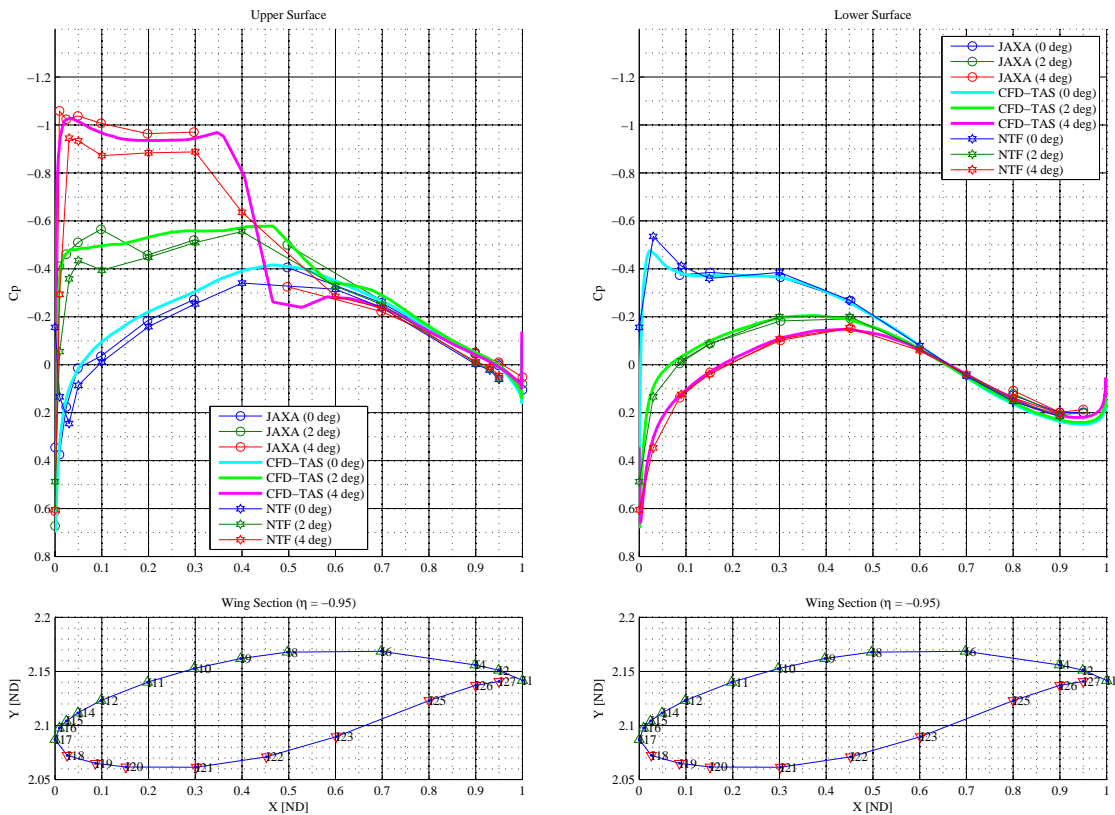


(b) With wing deformation correction.

**Figure 17. Pressure distribution at Section H.**



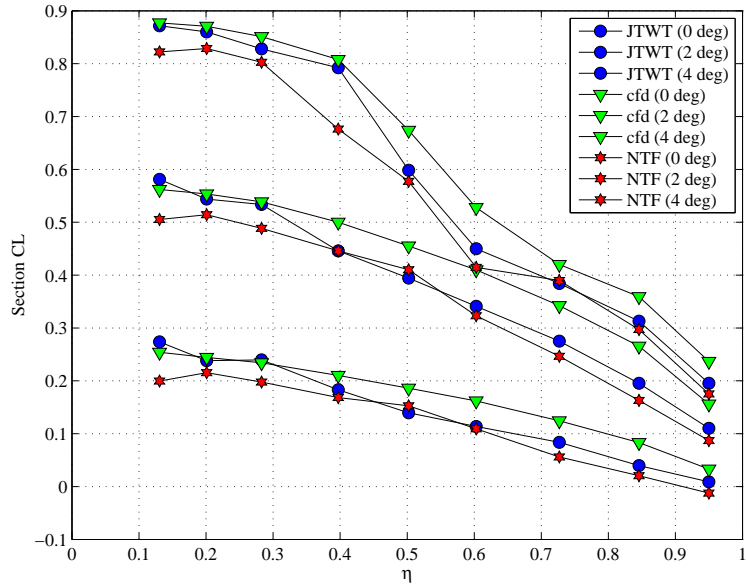
(a) Without wing deformation correction.



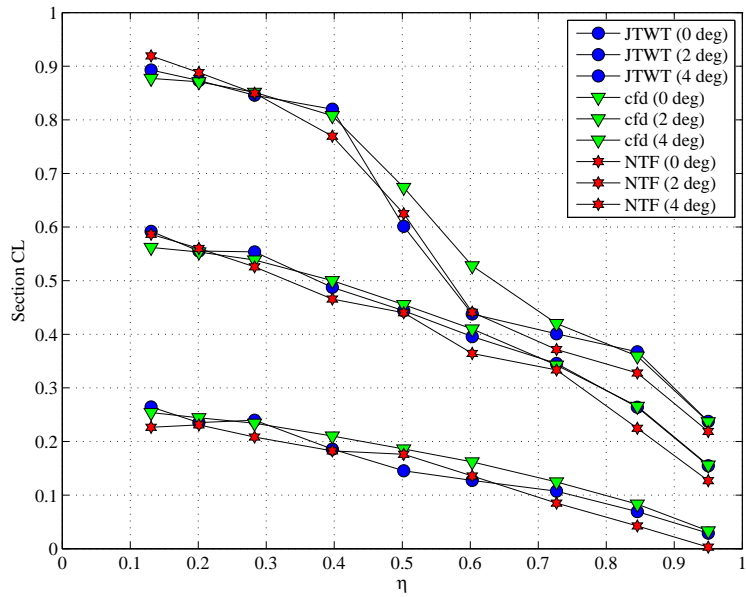
(b) With wing deformation correction.

Figure 18. Pressure distribution at Section I.

## A.B. Lift Distribution



(a) Without wing deformation correction.

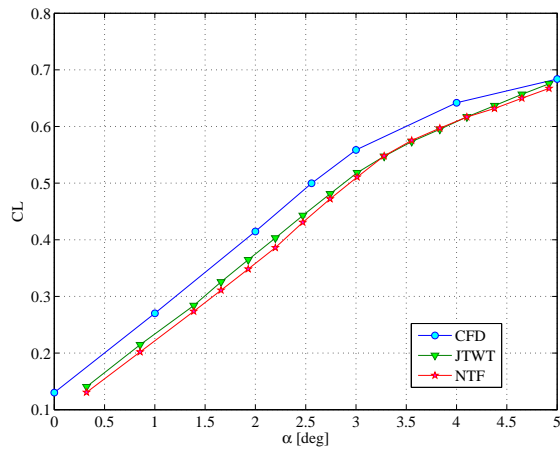


(b) With wing deformation correction.

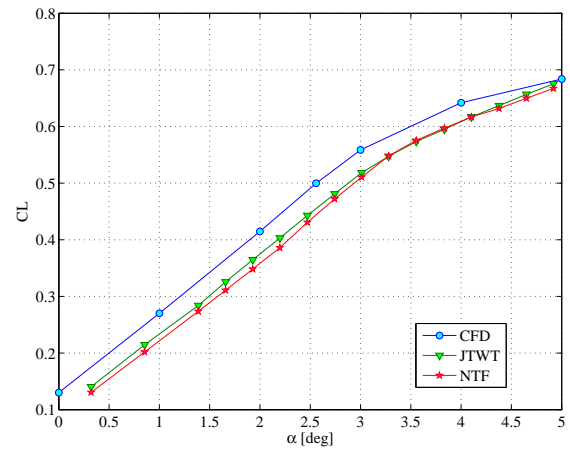
Figure 19. Lift distribution on the main wing including JTWT, CFD and NTF data.

## A.C. Force Coefficients

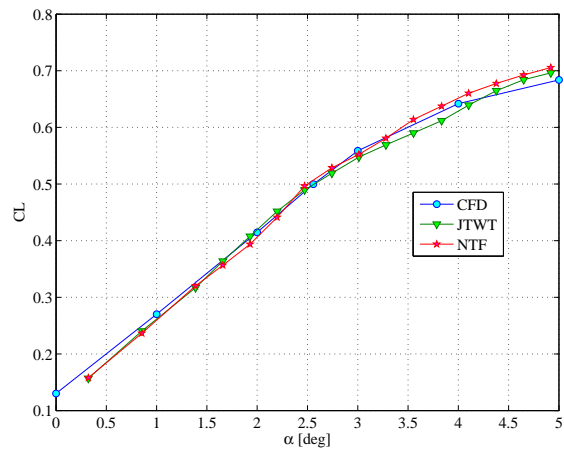
### A.C.1. $C_L$



(a) Neither with Reynolds number nor wing deformation correction.



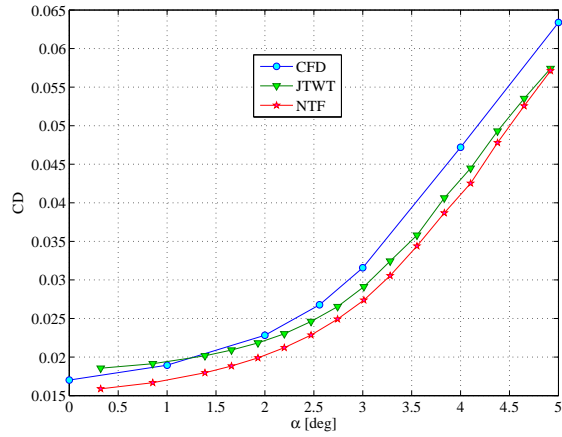
(b) With Reynolds number correction but not with wing deformation correction.



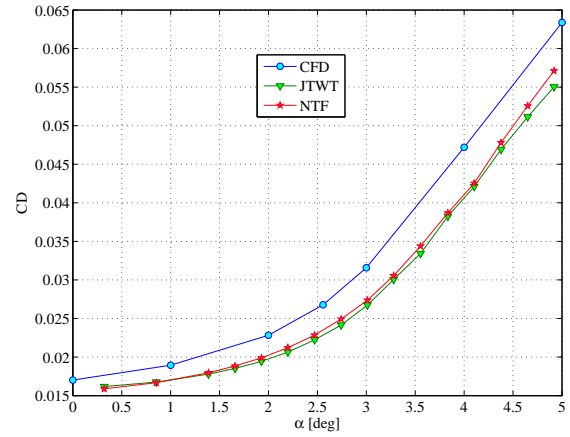
(c) With Reynolds number and wing deformation correction.

Figure 20.  $C_L$  vs  $\alpha$ .

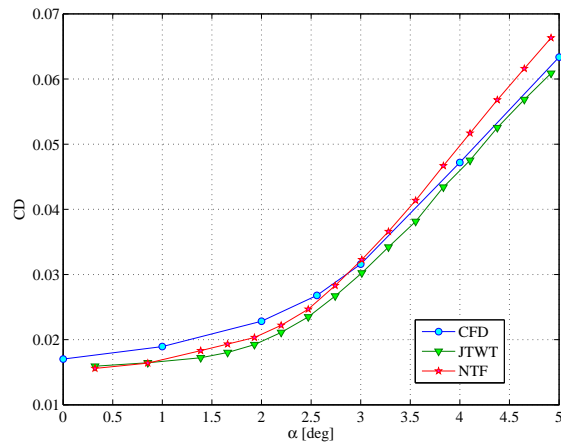
A.C.2.  $C_D$



(a) Neither with Reynolds number nor wing deformation correction.



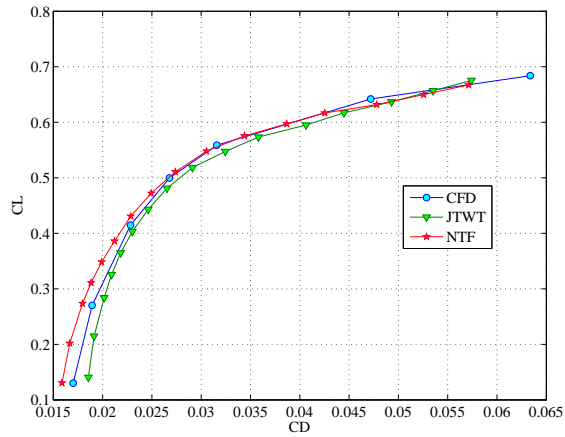
(b) With Reynolds number correction but not with wing deformation correction.



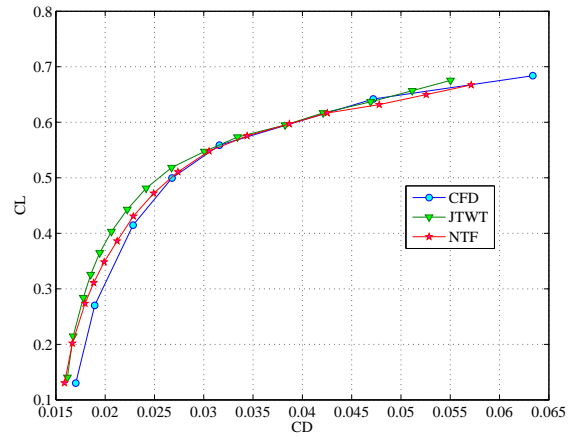
(c) With Reynolds number and wing deformation correction.

Figure 21.  $C_D$  vs  $\alpha$ .

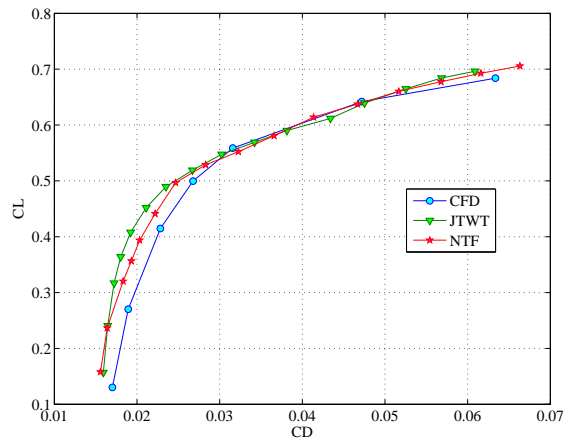
A.C.3. Drag Polar



(a) Neither with Reynolds number nor wing deformation correction.



(b) With Reynolds number correction but not with wing deformation correction.



(c) With Reynolds number and wing deformation correction.

Figure 22.  $C_L$  vs  $C_D$ .